Terra Nova

Post-impact event bed (tsunamite) at the Cretaceous–Paleogene boundary deposited on a distal carbonate platform interior

Journal:	*Terra Nova*
Manuscript ID	TER-2016-0078.R2
Wiley - Manuscript type:	Paper
Date Submitted by the Author:	n/a
Complete List of Authors:	Korbar, Tvrtko; Croatian Geological Survey, Department of Geology MacDonald, Iain; School of Earth, Ocean and Planetary Sciences, Cardiff University Premec Fućek, Vlasta; INA-Industrija nafte d.d., Exploration Sector Fuček, Ladislav; Croatian Geological Survey, Department of Geology Posilović, Hrvoje; Croatian Geological Survey, Department of Geology
Keywords:	Cretaceous-Paleogene boundary, asteroid impact, carbonate platform, event bed, tsunamite

Running head: K–Pg boundary event bed on carbonate platform

Post-impact event bed (tsunamite) at the Cretaceous–Paleogene boundary deposited on a distal carbonate platform interior

Tvrtko Korbar[1], Iain McDonald[2], Vlasta Premec Fućek[3], Ladislav Fuček[1], Hrvoje Posilović[1]

[1] Croatian Geological Survey, Department of Geology, Sachsova 2, HR-10000 Zagreb, Croatia.

[2] School of Earth, Ocean and Planetary Sciences, Cardiff University, Park Place, Cardiff CF10 3AT, United Kindom.

[3] INA-Industrija nafte d.d., Exploration Sector, Lovinčićeva 4, HR-10000 Zagreb, Croatia.

ABSTRACT

We show crucial evidence for the Cretaceous–Paleogene (K–Pg) boundary event recorded within a rare succession deposited in an inner-platform lagoon on top of a Mesozoic, tropical, intra-oceanic (western Tethys) Adriatic carbonate platform, that is exposed at Likva cove on the island of Brač (Croatia). The last terminal Maastrichtian fossils appear within a distinct 10-12 cm thick event bed that is characterized by soft-sediment bioturbation and rare shocked-quartz grains, and is interpreted as a distal tsunamite. Directly overlying this is 2 cm thick reddish-brown clayey mudstone containing planktonic foraminifera typical for the basal Danian, and with elevated platinum-group elements in chondritic proportions indicating a clear link to the Chicxulub asteroid impact. These results strongly support the first discovery of the "potential" K–Pg boundary tsunamite on the neighboring island of Hvar, and these two complementary sections represent probably the most complete record of the event among known distal shallow-marine successions.

Introduction

The Chicxulub asteroid impact (Alvarez *et al*., 1980; Smit and Hertogen, 1980; Schulte *et al*., 2010) triggered global mass extinctions and extraordinary sedimentary perturbations at the Cretaceous–Paleogene (K–Pg) boundary some 66 million years ago (Renne *et al*., 2013). Within distal sedimentary successions around the globe, the boundary is marked by a thin clay horizon containing elevated concentrations of platinum-group elements (PGE), along with shocked mineral grains and spherules from the impact fallout (e.g., Bohor and Izett, 1986; Alvarez *et al*., 1990; Smit, 1999; Montanari and Koeberl, 2000; Glass and Simonson, 2013). While deep-water successions have been extensively studied (Smit 1999; Klaus *et al*., 2000; Claeys *et al*., 2002; MacLeod *et al*., 2007; Esmeray-Senlet *et al*., 2015), including ichnofossils and discontinuities at the boundary (e.g., Rodríguez-Tovar and Uchman, 2008; Alegret *et al*., 2015), comparatively less is known about shallow-water perturbations in distal regions (Steuber and Schlüter, 2012). Although carbonate platform successions in the peri-Adriatic region (Fig. 1) commonly exhibit a hiatus that includes the K–Pg transition (Eberli *et al*., 1993; Bosellini *et al*., 1999; Vlahović *et al*. 2005; Korbar 2009), the boundary interval has recently been documented on the island of Hvar in Croatia (Korbar *et al*., 2015). The K–Pg boundary is tentatively indicated also within the Likva section on the neighboring island of Brač, but only negative evidence for the boundary has previously been reported for this site (Jelaska and Ogorelec, 1983; Gušić and Jelaska, 1990; Steuber *et al*., 2005). In this paper, we present a focused sedimentological, biostratigraphic, and geochemical study of the central part of the Likva section, including an exceptional occurrence of the impact ejecta and the K–Pg boundary "clay" containing isolated specimens of index planktonic foraminifera that are very rare within carbonate platform successions. Thus, the Likva section on Brač provides additional details missing in the "potential" K–Pg boundary tsunamite firstly discovered on the neighboring island of Hvar (Korbar *et al*., 2015),

Geological setting

The present-day peri-Adriatic area (central-northern Mediterranean) represents the deformed sedimentary cover of the Adriatic microplate or Adria – the Mesozoic northern promontory of Africa

(Channell *et al*., 1979). The Mesozoic Adriatic carbonate platform (ACP) was a low-latitude, mainly shallow-marine system comparable to the modern Bahama banks (Eberli *et al*., 1993; Vlahović *et al*., 2005), situated in the central part of Adria within central-western Tethys (Fig. 1). Cenozoic deformation of the Mesozoic platform carbonates was controlled by Alpine orogenesis, forming a complex fold-and-thrust belt of the External Dinarides along the northeast margin of the Adriatic Sea (Korbar 2009).

Material and methods

The island of Brač is built predominantly of ACP carbonates (Fig. S1) and the K–Pg succession is exposed at Likva cove (43.389˚ N, 16.460˚ E; Figs. S1 and S2). The succession is a few tens of meters thick and characterized by typical shallow-water carbonates of the Sumartin Formation, indicating inner-platform, peritidal depositional environments (Jelaska and Ogorelec, 1983; Gušić and Jelaska, 1990; Steuber *et al*., 2005).

The suspected K–Pg interval was logged, macroscopically analyzed in the field, and sampled (Fig. 2). Standard polished slabs and thin sections were used for petrographic and micropaleontological assessments, following Flügel (2010). Planktonic foraminifera were successfully isolated only from a softer sample of the K–Pg "clay" on the smallest sieve (45 μm), and photographed by scanning electron microscopy (SEM) at INA (Zagreb). Taxonomic classification of Paleocene planktonic foraminifera identified in this study follows the work of Olsson *et al*. (1999), and Koutsoukos (2014), as well as the planktonic foraminiferal biozonation of Wade *et al*. (2011).

Nine limestone samples (5-10 g in mass) were analyzed for PGE and gold at Cardiff University (UK) using nickel sulfide fire assay followed by Te co-precipitation and inductively coupled plasma mass spectrometry (ICP-MS) as described in McDonald and Viljoen (2006). Data are given in supplementary Table S1. Selected limestone samples were dissolved in 10% HCl. The quartz grains were etched with 10% HF for five to ten minutes, and were analyzed and photographed on SEM coupled with energy dispersive spectrometer at CGS (Zagreb).

Results

The uppermost Maastrichtian miliolid limestones at Likva (facies "2.6." of Jelaska and Ogorelec, 1983), the type level of *Fleuryana adriatica* (De Castro *et al*., 1994), are characterized in the topmost part by a 70 cm thick succession of skeletal-peloidal limestone lithotypes (the uppermost bed of the interval "C" of Steuber *et al*., 2005). The succession comprises 4 intervals (numbers 1-4 on Fig. 2A), separated by flat or undulating discontinuities. From the base upwards: 20 cm thick requieniid rudist floatstone of interval 1; 8-15 cm thick packstone of interval 2; 25-32 cm thick wackestone of interval 3; and 10-12 cm thick packstone-grainstone of interval 4. Interval 4 (Figs. 2B-D, S2B-C, S3) is a distinct single depositional unit that is directly overlain by 2 cm of reddish-brown clayey mudstone – equated with the K–Pg boundary "clay" (Fig. 2B).

Intervals 1-4 contain a diversified Maastrichtian benthic association, while rare planktonic foraminifera and pithonellid calcispheres are only found in the wackestones of interval 3 (Fig. 3A). Besides various miliolids, benthic foraminifera recognized in these limestones are: *Fleuryana adriatica*, *Laffitteina mengaudi*, *Bolivinopsis* sp., Discorbidae, Rotaliidae, Ophthalmidiidae, and Valvulinidae, along with Ostracoda, *Thaumatoporella parvovesiculifera*, and Charophyta (calcareous brackish algae). Sr isotope stratigraphy data of Steuber *et al*. (2005) confirm the terminal Maastrichtian age of interval 1 that contains the last appearance of requieniid rudists *Apricardia* sp., as well as the last appearance of rudists in life-position within the ACP succession. Interval 3 is indistinctly bioturbated, while the topmost few cm are characterized by irregular dark grey traces of intergranular infiltrations from above (Fig. 2A).

Interval 4 has an undulating lower boundary (Fig. S1C) and a discontinuous bioclastic lag composed of requieniid rudist bioclasts (up to 10 mm long, Figs. 2C, 3B), as well as dark grey intraclasts of wackestone that is similar to interval 3 (Fig. 2C). The fossil assemblage is the same as in the intervals below, with the addition of unusual calcitic spherules characterized by rough exterior and complex sparitic-micritic walls (40-60 μm in diameter, Figs. 2D, 3C). The spherules are sparsely distributed throughout the interval 4, along with very rare detrital quartz grains (up to 60 μm in diameter). Interval 4 is marked by distinct reddish-brown, tubular (2-3 mm in diameter) bioturbation (Figs. 2B, C, S3) filled by finer-grained peloidal-bioclastic wackestones containing microbioclasts and Maastrichtian benthic foraminifera (Fig. 2D). The color is dispersed around tiny darker reddish-brown micritic carbonate grains with iron oxides and traces of

iron phosphates that are irregularly distributed within the bioturbation. The HCl insoluble residuum of whole interval 4 rock contains dark grey organic matter, rare shocked quartz grains (30-100 μm in diameter displaying multiple sets of closely spaced planar deformation features (PDFs), some 40 grains per 1 dm^3 of limestone, Fig. 4), potassium feldspars, pyroxene (diopside), kaolinite and (mainly framboidal) pyrite.

The clayey mudstone directly overlying interval 4 contains ostracods (Fig. 3D) and rare tiny planktonic foraminifera typical for the indistinct basal Danian Zones P0-Pα (Fig. 5). PGE are highly enriched in the mudstone, with respect to the other limestones (Fig. 2A, Table S1). High temperature PGE (Os, Ir, Ru, and Rh) in both the clayey mudstone and interval 4 are nearly chondritic but [Pt/Ir]N, [Pd/Ir]N and [Au/Ir]N are suprachondritic (Table S1) reflecting a crustal PGE component (Koeberl *et al*. 2012). Hydrogen sulfide release during treatment with HCl indicated dissolution of sulfides (probably pyrite). The insoluble residuum consists of kaolinite and illite.

The overlying 6-8 cm thick mudstone (interval 5) is characterized by thalassinoid bioturbation, and contains ostracods, tiny planktonic foraminifera (tentatively Pα-P1a zones according to thin-section determination of *Subbotina* cf. *trivialis*, *Globanomalina* cf. *planocompressa*, and *Eoglobigerina* cf. *eobulloides*), and rare small benthic foraminifera (*Bangiana hanseni*, *Rotorbinella hermi*, *Laffitteina* sp., and tiny miliolids). The overlying >60 cm thick mudstone-wackestones of the intervals 6-8 are characterized by rare planktonic foraminifera and a gradual increase in diversity and proportion of benthic foraminifera, microgastropods, and Characean algae.

Discussion

This study shows that the uppermost Maastrichtian miliolid limestones in Likva cove on the island of Brač are characterized by polyspecific (predominantly benthic) communities, indicating a subtidal inner-platform environment that differs from the underlying intertidal laminites (Jelaska and Ogorelec, 1983). The presence of some brackish taxa (Characean algae) suggests at least occasional influence of fresh water, while rare planktonic foraminifera (Fig. 3A) and pithonellid calcispheres in interval 3 also indicate an influence from the open sea within what is interpreted as a semi-enclosed lagoon on top of a tide-dominated ACP interior. This association is unusual but in accordance with the most recent data on eustatic sea-level rise

134 during the latest Maastrichtian (Esmeray-Senlet *et al*., 2015), related to the increased SST that is recorded
135 even at high latitudes (Witts *et al*., 2016).

136 Considering the depositional setting, its distinctive appearance, erosional lower boundary, rip-up
137 clasts, and bioclastic lag, interval 4 could be interpreted as an event bed – possibly a distal carbonate
138 platform tsunamite rather than storm deposit (Morton *et al*., 2007), because even major storms are known to
139 have little impact on modern tide-dominated platform-top sedimentation (Boss *et al*., 1993; Rankey *et al*.,
140 2004). Thus, probably only a major tsunami surge, that can be considered as an extraordinary tide, is capable
141 to make such a distinct event bed within the platform interior on modern and ancient carbonate platforms
142 (see discussion in Korbar *et al*., 2015).

143 The complex calcitic spherules from interval 4 (Figs. 2D and 3C) do not resemble simple Late
144 Cretaceous marine pithonellid calcispheres found in interval 3, that are common also in open carbonate
145 platform facies of the ACP (e.g., Korbar *et al*., 2012). Interestingly, the spherules more closely resemble
146 Paleozoic calcispheres (cf. Plate 66/1-3 of Flügel, 2010) and Proterozoic impact spherules (cf. Fig. 7.8 of
147 Glass and Simonson, 2013). Although the original composition of impact spherules can be changed during
148 diagenesis (Montanari *et al*., 1983; Montanari, 1991), spherules from the event bed are probably of biogenic
149 origin, possibly fresh-water or hypersaline calcispheres displaced from a pond by the tsunami.

150 The slightly elevated Os, Ir and Ru concentrations in interval 4 are chondritic (Table S1), and given
151 the association with shocked quartz, support the idea of sparsely re-distributed and diagenetically altered
152 ejecta within the tsunamite. Similar PGE values are detected on top of the Majerovica K–Pg tsunamite on
153 the island of Hvar (Korbar *et al*., 2015) and likely represent the same depositional event. Majerovica is
154 currently situated 24 km south of Likva cove (Fig. S1), and probably >40 km 66 myr ago. Furthermore,
155 precise biostratigraphy of the directly overlying K–Pg "clay" with its chondritic PGE (Fig. 2A, Table S1),
156 strongly supports direct correlation between the two sites and with the K–Pg trans-Atlantic tsunami triggered
157 by the Chicxulub impact (Norris *et al*., 2000; MacLeod *et al*., 2007; Korbar *et al*., 2015).

158 The truly global significance of the K–Pg boundary in the Likva section, however, comes from the
159 sedimentary structures and the microfossils that are preserved. Smooth edges and morphology of the
160 bioturbation in interval 4 suggest soft-sediment burrowing by annelid worms – polychaetes (Herringshaw *et*

161 *al*., 2010), while finer-grained infill and non-carbonate minerals suggest changes of physical and
162 geochemical characters of the pristine deposit. According to studies on modern analogues, polychaetes are
163 the most abundant benthic non-skeletal macrofauna in tropical, shallow-water, intraoceanic carbonate
164 sediments, especially in lagoons (e.g., Frouin and Hutchings, 2001). Most polychaetes are non-selective
165 surface deposit feeders that ingest marine sediment, and the processing time for the sediment can be as little
166 as 15 minutes (Rouse and Pleijel, 2001). However, some annelids are selective deposit feeders that seek
167 particles of a specific size, and their processing time may cover 2-2.5 hours (Bock and Miller, 1999).
168 Importantly, decay of sediment particles processed by the deposit-feeding organisms is faster because of
169 digestion (Needham et al., 2004).

170 The Chicxulub impact ejecta layer is fairly uniform in thickness (2-3 mm) at distances of 7000–
171 11000 km (Smit, 1999). Ballistic and most of relatively coarser-grained non-ballistically distributed impact
172 ejecta probably reached the most globally distal sites within several hours (Artemieva and Morgan, 2009),
173 while the post-impact landslide tsunami likely took 10-20 hours to reach the ACP (Fig. 1; Norris *et al*.,
174 2000; Ward, 2001; Korbar *et al*., 2015).The expected delay between arrival of ballistic ejecta and the
175 tsunami was probably long enough for the deposit-feeding polychaetes to ingest some of the deposited ejecta
176 particles of the optimal size (Bock and Miller, 1999). Following the surge of the very distal and attenuated
177 tsunami over the ACP top, and deposition of 10-12 cm thick tsunamite in the lagoon, passively transported
178 and temporarily buried animals would attempt to escape from the relatively thick sand blanket. Intensive
179 burrowing by polychaetes during the hours to days after the deposition (Herringshaw *et al*., 2010) is a
180 probable cause of a lack of an expected thin mudcap from the uppermost part of the deposit. Ingested
181 ballistic ejecta could be reworked along with later non-ballistic, early deposited impact dust from the top of
182 the tsunamite into the burrows to produce Os, Ir, and Ru, enrichment in interval 4 . The clay minerals could
183 originate from ejecta, degraded firstly during digestion (Needham *et al*., 2004), and subsequently during
184 diagenesis (Montanari, 1991).

185 The K–Pg "clay" (Fig. 2B), i.e., lime mud mixed with settling impact dust and aerosols, was
186 deposited in the lagoon during the sudden decrease in carbonate production, which lasted decades to
187 millennia, as a result of a global "impact-winter" (Galeotti *et al*., 2004; Vellekoop *et al*., 2014).

Nevertheless, that 2-cm thick horizon had to be deposited during the time needed for evolution of new species of planktonic foraminifera (Fig. 5) defining the first Danian Zones P0 and Pα, i.e. during at least the first ten millennia of the Cenozoic (Koutsoukos, 2014). Increasing abundance and variability of benthic fossils in mudstones of the interval 5, tentatively assigned to the zones Pα-P1a, suggest that shallow-water carbonate factory recovered during the next few tens of thousands years (Wade *et al*., 2011).

Conclusions

The tsunamite at Likva represents probably the most distal reported sedimentary record of the K–Pg boundary tsunami that is much thinner but more complete than at Majerovica (Korbar *et al*., 2015). These two sections together strongly support the hypothesis about the K–Pg boundary tsunami on the ACP.

Environmental effects in the marine realm in the immediate aftermath of the Chicxulub impact are incompletely recorded in many of the well-known distal deep-water K–Pg boundary sections around the world (Claeys *et al*., 2002; Schulte *et al*., 2010), because of a slow settling of the ejecta through the water column (Stokes's Law), discontinuities in the sedimentary record (Alegret *et al*., 2015), and the absence of the tsunami reworking (Smit, 1999). In contrast, shallow-water successions can preserve evidence for the first hours following impact, especially shallow-marine (sub)tropical carbonates because of early cementation. However, shallow-water deposits are also more prone to subsequent reworking or erosion, and the exceptional preservation found at Likva offers an important new opportunity for further research into the both immediate aftermath one of the most catastrophic global events in Earth's history, and a recovery of a carbonate factory at the beginning of Cenozoic.

Acknowledgements

We thank to Renata Slavković for SEM images of planktonic foraminifera, Katica Drobne for determination of some Paleocene benthic foraminifera, and Alessandro Montanari for a previous fruitful discussion on the topic and some suggestions for the methodology. We thank also to the Editors as well as to Bruce M. Simonson, Francisco J. Rodríguez-Tovar, R. Mark Leckie, and an anonymous reviewer for their constructive reviews.

References

Alegret, L., Rodríguez-Tovar, F.J., and Uchman, A., 2015. How bioturbartion obscured the Cretaceous–Paleogene boundary record. *Terra Nova*, **27**, 225-230.

Alvarez, L.W., Alvarez, W., Asaro, F., and Michel, H.V., 1980. Extraterrestrial cause for the Cretaceous-Tertiary extinction. *Science*, **208**, 1095-1108.

Alvarez, W., Asaro, F., and Montanari, A., 1990. Ir profile for 10 Myr across the Cretaceous-Tertiary boundary at Gubbio (Italy). *Science*, **250**, 1700-1702.

Artemieva N., and Morgan J., 2009. Modeling the formation of the K Pg boundary layer. *Icarus*, **201**, 768-780.

Bock, M.J. and Miller, D.C., 1999. Particle selectivity, gut volume, and the response to a step change in diet for deposit feeding polychaetes. *Limnol. Oceanogr.*, **44**, 1132-1138.

Bohor, B.F., and Izett, G., 1986. Worldwide size distribution of shocked quartz at the K/T boundary: Evidence for a North American impact site. *Lunar Planet. Sci.*, **17**, 68-69.

Bosellini, A., Morsilli, M., and Neri, C., 1999. Long-term event stratigraphy of the Apulia platform margin (Upper Jurassic to Eocene, Gargano, southern Italy). *J. Sed. Res.*, **69**, 1241-1252.

Boss, S.K., and Neumann, A.C., 1993. Impacts of Hurricane Andrew on carbonate platform environments, north Great Bahama Bank. *Geology*, **21**, 897-900.

Channell, J.E.T., D'Argenio, B., and Horvath, F., 1979. Adria, the African promontory, in Mesozoic Mediterranean palaeogeography. *Earth-Sci. Rev*, **15**, 213-292.

Claeys, P.H., Kiessling, W., and Alvarez, W., 2002. Distribution of Chicxulub ejecta at the Cretaceous-Tertiary boundary. In: *Catastrophic Events and Mass Extinctions: Impacts and Beyond* (C.,Koeberl and K.G. MacLeod, eds). *Geol. Soc. America Spec. Paper*, **356**, 55-68.

De Castro, P., Drobne, K., and Gušić, I., 1994. *Fleuryana adriatica* n. gen., n. sp. (Foraminiferida) from the uppermost Maastrichthian of the Brač island (Croatia) and some other localities on the Adriatic carbonate platform. *Rasprave IV. razreda SAZU* (Ljubljana), **35**, 129-149.

Eberli, G.P., Bernoulli, D., Sanders, D., and Vecsei, A., 1993. From aggradation to progradation: the Maiella platform (Abruzzi, Italy). In: *Cretaceous carbonate platforms* (A.J. Simo, R.W. Scott, and J.-P. Masse, eds). *Mem. American Assoc. Petrol. Geol.*, **56**, 213-232.

Esmeray-Senlet, S., Özkan-Altiner, S., Altiner, D., and Miller, K.G., 2015. Planktonic foraminiferal biostratigraphy, microfacies analysis, sequence stratigraphy, and sea-level changes across the Cretaceous–Paleogene boundary in the Haymana basin, central Anatolia, Turkey. *J. Sed. Res.*, **85**, 489-508.

Flügel, E., 2010. Microfacies of Carbonate Rocks: Heidelberg, Springer, 984 pp.

Frouin, P., and Hutchings, P., 2001. Macrobenthic communities in a tropical lagoon (Tahiti, French polynesia, central Pacific). *Coral Res*., **19**, 277-285.

Galeotti, S., Brinkhuis, H., and Huber, M., 2004. Records of postCretaceous-Tertiary boundary millennial-scale cooling from the western Tethys: A smoking gun for the impact-winter hypothesis? *Geology*, **32**, 529-532.

Glass, B.P., and Simonson, B.M., 2013. Distal Impact Ejecta Layers. In: *Impact Studies* (C. Koeberl, ed). Heidelberg, Springer, 716 pp.

Gušić, I., and Jelaska, V., 1990. Stratigrafija gornjokrednih naslaga otoka Brača u okviru geodinamske evolucije Jadranske karbonatne platforme (Upper Cretaceous stratigraphy of the Island of Brač within the geodynamic evolution of the Adriatic carbonate platform). *Djela Jugoslavenske akademije znanosti i umjetnosti* (Zagreb), **69**, 160 pp.

Herringshaw, L.G., Sherwood, O.A., and McIlroy, D., 2010. Ecosystem engineering by bioturbating polychaetes in event bed microcosms. *Palaios*, **25**, 46-58.

Jelaska, V., and Ogorelec, B., 1983. The Upper Cretaceous depositional dnvironments of the carbonate platform on the Island of Brač (Stop 10). In: *Contribution to Sedimentology of Some Carbonate and Clastic Units of Coastal Dinarides* (LJ. Babić, and V. Jelaska, eds). 4th I.A.S. regional meeting, Split, Excursion Guide-book, 99-124.

Klaus, A., Norris, R.D., Kroon, D., and Smit, J., 2000. Impact-induced K-T boundary mass wasting across the Blake Nose, W. North Atlantic. *Geology*, **28**, 319-322.

Koeberl, C., Claeys, P., Hecht, L., and McDonald, I., 2012. Geochemistry of impacts. *Elements*, **8**, 37-42.

Korbar, T., 2009. Orogenic evolution of the External Dinarides in the NE Adriatic region: A model constrained by tectonostratigraphy of Upper Cretaceous to Paleogene carbonates. *Earth-Sci. Rev.*, **96**, 296-312.

Korbar, T., Glumac, B., Cvetko Tešovic, B., and Cadieux, S.B., 2012. Response of a carbonate platform to the Cenomanian-Turonian drowning and OAE2: A case study from the Adriatic Platform (Dalmatia, Croatia). *J. Sed. Res.*, **82**, 163-176.

Korbar, T., Montanari, A., Premec Fućek, V., Fuček, L., Coccioni, R, McDonald, I, Claeys, P., Schulz, T., and Koeberl, C., 2015. Potential Cretaceous-Paleogene boundary tsunami deposit in the intra-Tethyan Adriatic Carbonate Platform section of Hvar (Dalmatia, Croatia). *Geol. Soc. America Bull.*, **127**, 1666-1680.

Koutsoukos, E.A.M., 2014. Phenotypic plasticity, speciation, and phylogeny in early Danian planktic foraminifera. *J. Foram. Res.*, **44**, 109-142.

MacLeod, K.G., Whitney, D.L., Huber, B.T., and Koeberl, C., 2007. Impact and extinction in remarkably complete Cretaceous-Tertiray boundary sections from Demerara Rise, tropical western North Atlantic. *Geol. Soc. America Bull.*, **119**, 101-115.

McDonald, I., and Viljoen, K.S., 2006. Platinum-group element geochemistry of mantle eclogites: a reconnaissance study of xenoliths from the Orapa kimberlite, Botswana. *Appl. Earth Sci.* (*Trans. Inst. Min. Metall. B*), **115**, B81-93.

Montanari, A., 1991. Authigenesis of impact spheroids in the K/T boundary clay from Italy: new constraints for high-resolution stratigraphy of terminal Cretaceous events. *J. Sediment. Petrol*., **61**, 315-339.

Montanari A., and Koeberl, C., 2000. Impact stratigraphy: The Italian record: Heidelberg, Springer, 364 Pp.

Montanari A., Hay R.L., Alvarez W., Asaro F., Michel H.V., Alvarez L.W., and Smit J., 1983. Spheroids at the Cretaceous-Tertiary boundary are altered impact droplets of basaltic composition. *Geology*, **11**, 668-671.

Morton, R.A., Gelfenbaum, G., and Jaffe, B.E., 2007. Physical criteria for distinguishing sandy tsunami and storm deposits using modern examples: *Sed. Geol*., **200**, 184-207.

Needham, S.J., Worden, R.H., and McIlroy, D., 2004. Animal-sediment interactions: The effect of ingestion and excretion by worms on mineralogy. *Biogeosciences*, **1**, 113-121.

Norris, R.D., Firth, J., Blusztajn, J., and Ravizza, G., 2000. Mass failure of the North Atlantic margin triggered by the Cretaceous/Paleogene bolide impact. *Geology*, **28**, 1119-1122.

Olsson, R.K., Hemleben, C., Berggren, W.A., and Huber, B.T., 1999. Atlas of Paleocene planktonic foraminifera. Smithsonian Contributions to Paleobiology, **85**, 252 pP.

Rankey, E.C., Enos, P., Steffen, K., and Druke, D., 2004. Lack of impact of Hurricane Michelle on tidal flats, Andros Island, Bahamas: Integrated remote sensing and field observations. *J. Sed. Res*., **74**, 654-661.

Renne, P.R., Deino, A.L., Hilgen, F.J., Kuiper, K.F., Mark, D.F., Mitchell III, W.S., Morgan, L.E., Mundil, R., and Smit, J., 2013. Time scales of critical events around the Cretaceous-Paleogene Boundary. *Science*, **339**, 684-687.

299 Rodríguez-Tovar, F.J., and Uchman, A., 2008. Bioturbational disturbance of the Cretaceous–Palaeogene (K–Pg)
300 boundary layer: Implications for the interpretation of the K–Pg boundary impact event: *Geobios*, **41**, 661–667.
301 Rouse, G.W., and Pleijel, F., 2001. Polychaetes. Oxford University Press, 349 pp.
302 Smit, J., 1999, The global stratigraphy of the Cretaceous-Tertiary boundary impact ejecta: *Ann. Rev. Earth and Planet.*
303 *Sci.*, **27**, 75-113.
304 Smit, J., and Hertogen, J., 1980. An extraterrestrial event at the Cretaceous-Tertiary boundary. *Nature*, **28**, 198-200.
305 Schulte, P., Alegret, L., Arenillas, I., Arz, J.A., Barton, P.J., Brown, P.R., Bralower, T.J., Christeson, G.L., Claeys, P.,
306 Cockell, C.S., Collins, G.S., Deutsch, A., Goldin, T.J., Goto, K., Grajales-Nishimura, J.M., Grieve, R.A.F.,
307 Gulick, S.P.S., Johnson, K.R., Kiessling, W., Koeberl, C., Kring, D.A., Macleod, K.G., Matsui, T., Melosh, J.,
308 Montanari, A., Morgan, J.V., Neal, C.R., Nichols, D.J., Norris, R.D., Pierazo, E., Ravizza, G., Rebolledo-
309 Vieyra, M., Reimond, W.U., Robin, E., Salge, T., Speijer, R.P., Sweet, A.R., Urrutia-Fucugauchi, J., Vajda, V.,
310 Whalen, M.T., and Willumsen, P.S., 2010. The Chicxulub asteroid impact and mass extinction at the
311 Cretaceous-Paleogene Boundary. *Science*, **327**, 1214-1218.
312 Scotese, C.R., and Dreher, C., 2012. Global Geology. http://www.globalgeology.com/
313 Steuber, T., and Schlüter, M., 2012. Strontium-isotope stratigraphy of Upper Cretaceous rudist bivalves: Biozones,
314 evolutionary patterns and sea-level change calibrated to numerical ages. *Earth-Sci. Rev*, **114**, 42-60.
315 Steuber, T., Korbar, T., Jelaska, V., and Gušić, I., 2005. Strontium-isotope stratigraphy of Upper Cretaceous platform
316 carbonates of the Island of Brač (Adriatic Sea, Croatia): Implications for global correlation of platform
317 evolution and biostratigraphy. *Cretac. Res*., **26**, 741-756.
318 Vellekoop, J., Sluijs, A., Smit, J., Schouten, S., Weijers, J.W.H., Sinninghe Damsté, J.S., and Brinkhuis, H., 2014.
319 Rapid short-term cooling following the Chicxulub impact at the Cretaceous–Paleogene boundary. *Proc. Nat. Ac.*
320 *Sci.* **111**, 7537-7541.
321 Vlahović, I., Tišljar, J., Velić, I., and Matičec, D., 2005. Evolution of the Adriatic Carbonate Platform:
322 Palaeogeography, main events and depositional dynamics. *Palaeogeogr. Palaeoclimatol. Palaeoecol*., **220**, 333-
323 360.
324 Wade, B.S., Pearson, P.N., Berggren, W.A., and Palike, H., 2011. Review and revision of Cenozoic tropical
325 planktonic foraminiferal biostratigraphy and calibration to the geomagnetic polarity and astronomical time
326 scale. *Earth-Sci. Rev*, **104**, 111-142.
327 Ward, S.N., 2001. Landslide Tsunami. *J. Geoph. Res*., **106**, 11201-11215.

Witts, J.D., Whittle, R.J., Wignall, P.B., Crame, J.A., Francis, J.E, Newton, R.J., and Bowman, V.C., 2016. Macrofossil evidence for a rapid and severe Cretaceous–Paleogene mass extinction in Antarctica. *Nat. Commun*. **7**:11738, doi: 10.1038/ncomms11738

.

FIGURE CAPTIONS

Fig. 1 Simplified Cretaceous–Paleogene (K–Pg) paleogeography showing Chicxulub impact site (red circles), hypothetical traces of east propagated intercontinental tsunami (white broken lines), and Likva locality (red arrow) on the Adriatic Carbonate Platform (modified from Korbar *et al*., 2015 according to Scotese and Dreher, 2012). Brown – land, light blue – neritic, dark blue – bathyal and abyssal.

Fig. 2 (A) Outcrop photograph and simple stratigraphic column of the Cretaceous–Paleogene (K–Pg) boundary succession within a middle part of Sumartin Formation at Likva cove, showing intervals and obtained concentrations of PGEs and gold (numbers in small frames on the photograph mark exact position of the PGE samples, Table S1). (B) The reddish-brown K–Pg boundary clayey mudstone ("clay") contains planktonic foraminifera typical for basal Danian P0-Pα zones (see Fig. 5). The underlying event bed (Interval 4) contains the last appearance of Maastrichtian fossils, and is characterized by small intraclasts (arrow) ripped-up from the directly underlying wackestone of the interval 3, and rudist bioclasts in the lower part, along with distinct reddish-brown soft-sediment bioturbation throughout. The overlying Danian mudstone (Interval 5) contains ostracods (Fig. 3D) and rare Paleocene planktonic (Fig. 5) and benthic foraminifera (see text). Small rectangles mark position of photomicrographs shown in Fig. 3. (C) polished slab of Interval 4. (D) Photomicrograph showing oblique section of 2-mm wide burrow filled with finer-grained skeletal-microbioclastic wackestone containing Maastrichtian benthic foraminifer *Fleuryana adriatica*. Inset shows a magnification of one of calcispheres sparsely distributed throughout Interval 4 (see also Fig. 3C).

Fig. 3 Thin-section photomicrographs (positions marked by small rectangles in Fig. 2B) of the K–Pg boundary shallow-marine limestones at Likva. (A) Skeletal-peloidal wackestone from the topmost part of Interval 3 containing abundant benthic foraminifera, ostracods, and Charophyta skeletal remains, as well as rare Maastrichtian planktonic foraminifera and pithonellid calcispheres. Inset shows a magnified planktonic foraminifera *Rugoglobigerina* sp. from the central part (dashed frame) . (B) A bioclastic lag at the lowermost part of the event bed (Interval 4) composed of requieniid rudists. (C) Skeletal-peloidal packstone-grainstone from the central part of the K–Pg event bed. Inset shows unusual calcispheres from the central part (dashed frame). (D) Clayey mudstone (K–Pg "clay") with ostracods that contains tiny planktonic foraminifera shown on Fig. 5.

Fig. 4 SEM images (A-D) of shocked quartz grains showing closely spaced (<2 microns) planar deformation features (PDFs) and EDS spectra showing their composition. Grains shown in (B) and (C) display multiple sets of PDFs. Insoluble residuum of the K–Pg event bed (Interval 4).

Fig. 5 SEM images of the basal Paleocene (P0-Pα zones) planktonic foraminifera isolated from the K–Pg boundary "clay" of the Likva section (see Fig. 2). (A-B) *Guembelitria cretacea* CUSHMAN. (C) *Parvularugoglobigerina* cf. *longiapertura* BLOW. (D) *Eoglobigerina eobulloides* (MOROZOVA). (E) *Woodringina claytonensis* LOEBLICH and TAPPAN. (F) *Parvularugoglobigerina* cf. *extensa* (BLOW). (G-I) *Praemurica taurica* (MOROZOVA). (J-K) *Globoconusa daubjergensis* (BRÖNNIMANN). (L) *Chiloguembelina* cf. *morsei* (KLINE). Scale bars 20 μm.

Supporting information

Fig. S1 Overview geological map showing locations of the K–Pg boundary sections at Likva (Brač island, this paper) and Majerovica (Hvar island, Korbar et al., 2015). Green – Cretaceous to Paleocene platform carbonates. Orange – Eocene carbonates and clastics. Dotted black lines – regional unconformity. Red comb

382 line – major thrust fault. Small black comb symbol - bed strike and dip.

383

384 **Fig. S2 (A-C)** The outcrop photographs of the Cretaceous–Paleogene (K–Pg) succession on western coast
385 of the Likva cove (the island of Brač, Adriatic Sea, Dalmatia, Croatia).

386

387 **Fig. S3** The upper bedding surface of the K–Pg boundary event bed (Interval 4) showing distinct reddish-
388 brown soft-sediment bioturbation. Coastal outcrop 200 m west of Likva cove (the island of Brač, Adriatic
389 Sea, Dalmatia, Croatia). Coin diameter is 24 mm.

390

391 **Table S1.** Platinum-group elements (PGE) and gold (Au) concentrations in limestone samples from the K–
392 Pg boundary Likva section (Fig. 2A) and chondrite normalization chart.

393

394

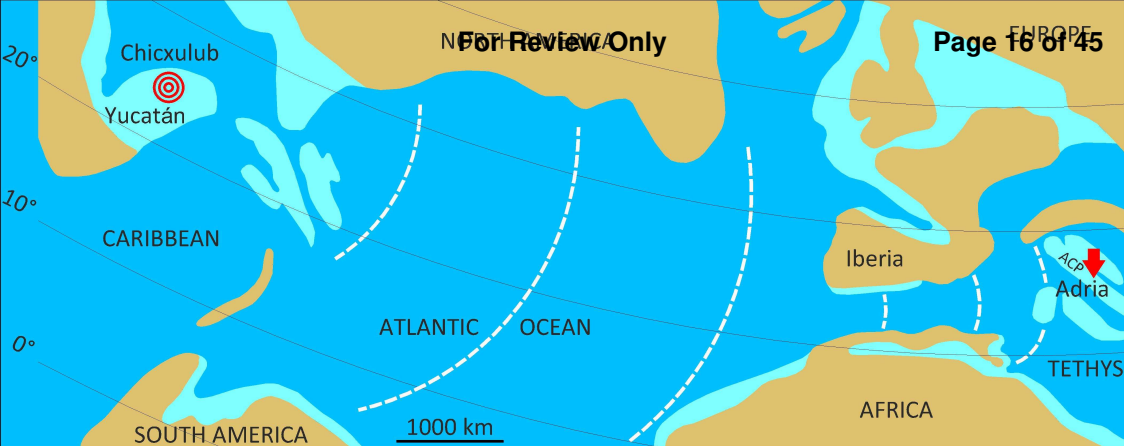
NORTH AMERICA
EUROPE
Chicxulub
Yucatán
20°
10°
0°
CARIBBEAN
ATLANTIC OCEAN
Iberia
ACP
Adria
TETHYS
AFRICA
SOUTH AMERICA
1000 km

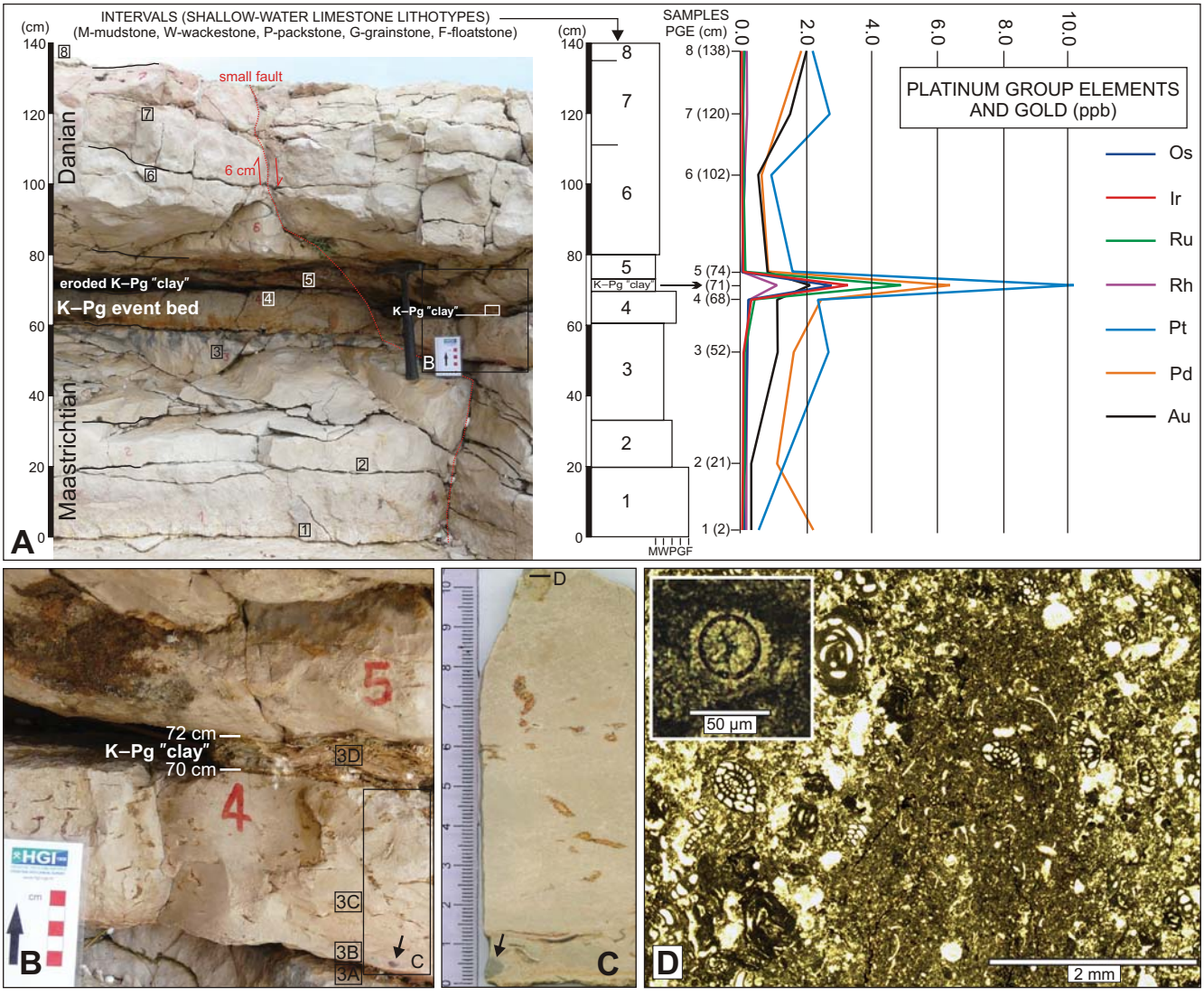
INTERVALS (SHALLOW-WATER LIMESTONE LITHOTYPES)
(M-mudstone, W-wackestone, P-packstone, G-grainstone, F-floatstone)
SAMPLES
PGE (cm)
PLATINUM GROUP ELEMENTS AND GOLD (ppb)
Os
Ir
Ru
Rh
Pt
Pd
Au
Danian
Maastrichtian
small fault
6 cm
eroded K–Pg "clay"
K–Pg event bed
K–Pg "clay"
72 cm
K–Pg "clay"
70 cm
50 µm
2 mm
MWPGF
A
B
C
D

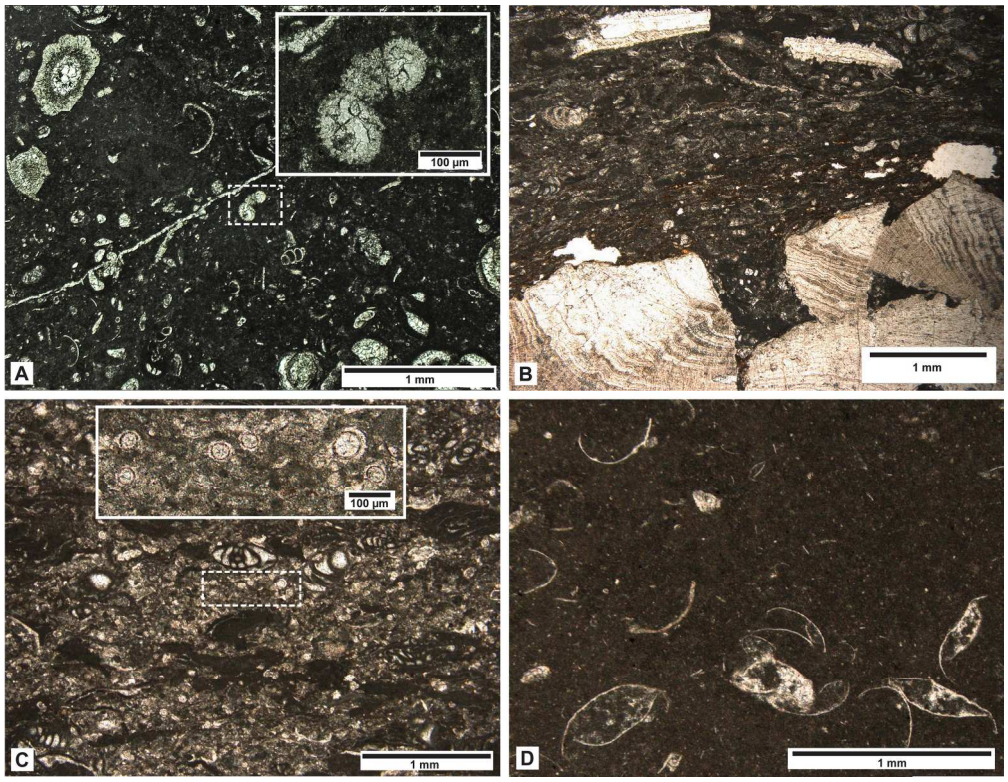

Fig. 3

180x138mm (300 x 300 DPI)

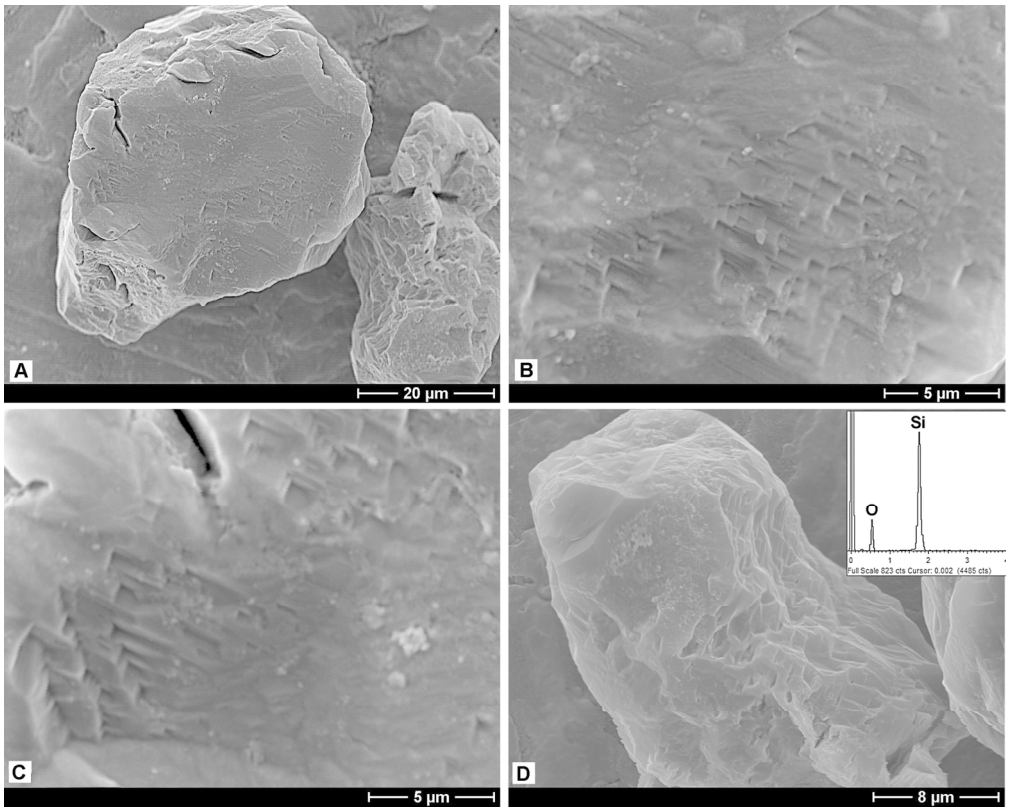

Fig. 4

144x115mm (300 x 300 DPI)

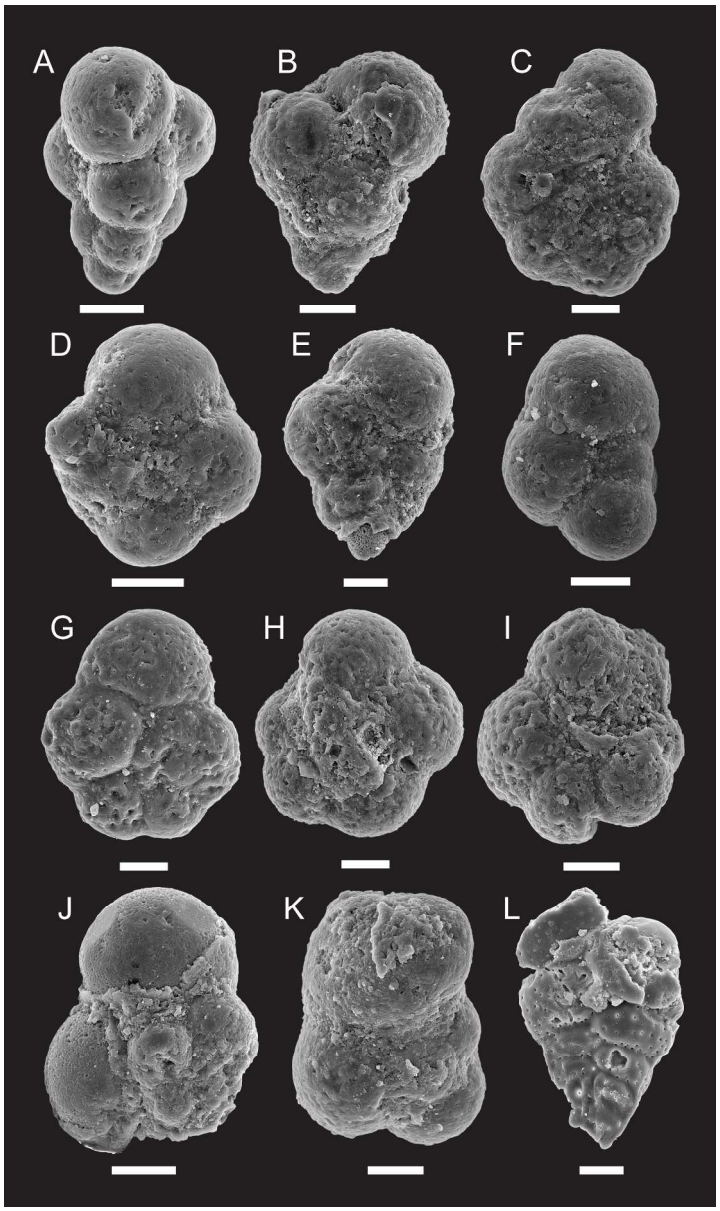

Fig. 5

156x263mm (300 x 300 DPI)

What follows is supplementary material, which will be made available online but will not appear in the print version.

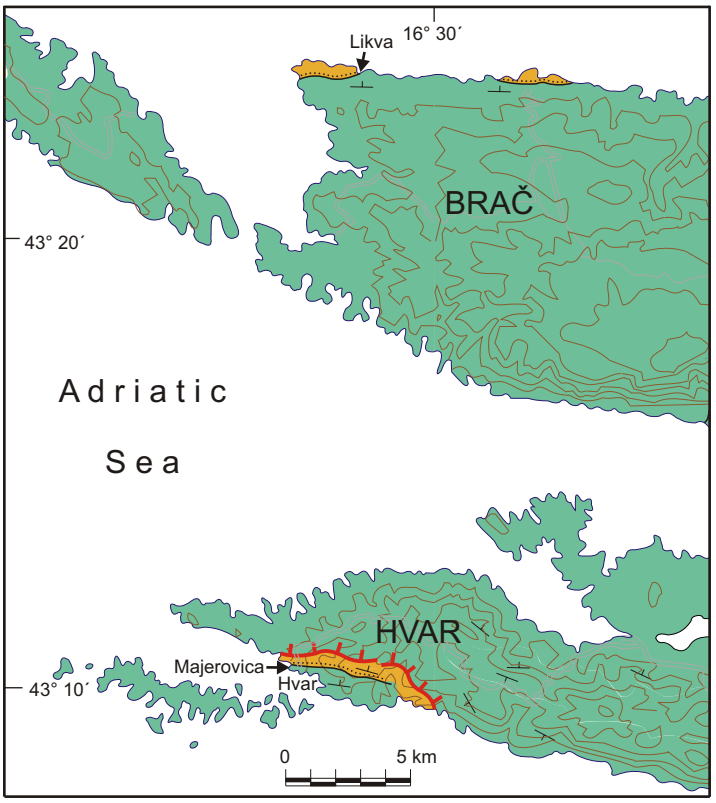
16° 30´
Likva
BRAČ
43° 20´
Adriatic
Sea
HVAR
Majerovica
Hvar
43° 10´
0
5 km


M A A S T R I C H T I A N
D A N I A N
K-Pg boundary


K-Pg boundary
event bed


K-Pg event bed

1151x649mm (72 x 72 DPI)

Blank corrected concentrations (ppb)

	Os	Ir	Ru	Rh	Pt	Pd	Au
Int-1	0,02	0,03	0,10	0,10	0,58	2,24	0,35
Int-2	0,09	0,07	0,09	0,14	1,35	1,11	0,30
Int-3	0,04	0,03	0,10	0,11	2,71	1,70	1,16
Int-4	0,39	0,34	0,46	0,18	2,52	2,58	1,04
K-Pg clay	2,86	3,27	4,80	1,03	10,06	6,37	2,12
Int-5	0,09	0,08	0,15	0,08	1,59	0,83	0,80
Int-6	0,10	0,08	0,17	0,07	0,95	0,67	0,56
Int-7	0,17	0,12	0,16	0,16	2,66	1,27	1,48
Int-8	0,06	0,08	0,14	0,20	2,27	1,87	2,02

Blanks

	Os	Ir	Ru	Rh	Pt	Pd	Au
Blank-A	<0.02	<0.01	0,07	<0.02	0,27	0,24	0,13
Blank-B	<0.02	<0.01	<0.05	0,05	0,32	0,30	0,21

Certified reference materials

	Os	Ir	Ru	Rh	Pt	Pd	Au
TDB1	0,07	0,12	0,26	0,65	5,48	23,6	6,71
WPR1	11,4	14,3	21,8	12,8	274	228	41,1
WMG1	22,3	48,0	30,0	25,9	748	382	116

Certified reference materials (Expected values)

	Os	Ir	Ru	Rh	Pt	Pd	Au
TDB1	0,1	0,15	0,3	0,7	5.8 +/- 1.1	22.4 +/- 1.4	6.3 +/- 1.0
WPR1	11,5	13,5	22	13,4	285	235	43
WMG1	24,1	46,4	34,7	26,3	731	382	110

Samples were prepared by nickel sulfide fire assay with Te co-precipitation. PGE and Au were determined by ICP-MS. Full methodology is given in:

Huber et al. (2001) Geochemistry and petrology of Witwatersrand and Dwyka diamictites from South Africa: search for an extraterrestrial component: Geochimica et Cosmochimica Acta, v. 65, p. 2007-2016.

McDonald and Viljoen (2006) Platinum-group element geochemistry of mantle eclogites: a reconnaissance study of xenoliths from the Orapa kimberlite, Botswana. Appl. Earth Science (Trans. Inst. Min. Metall. B), 115, B81-93.

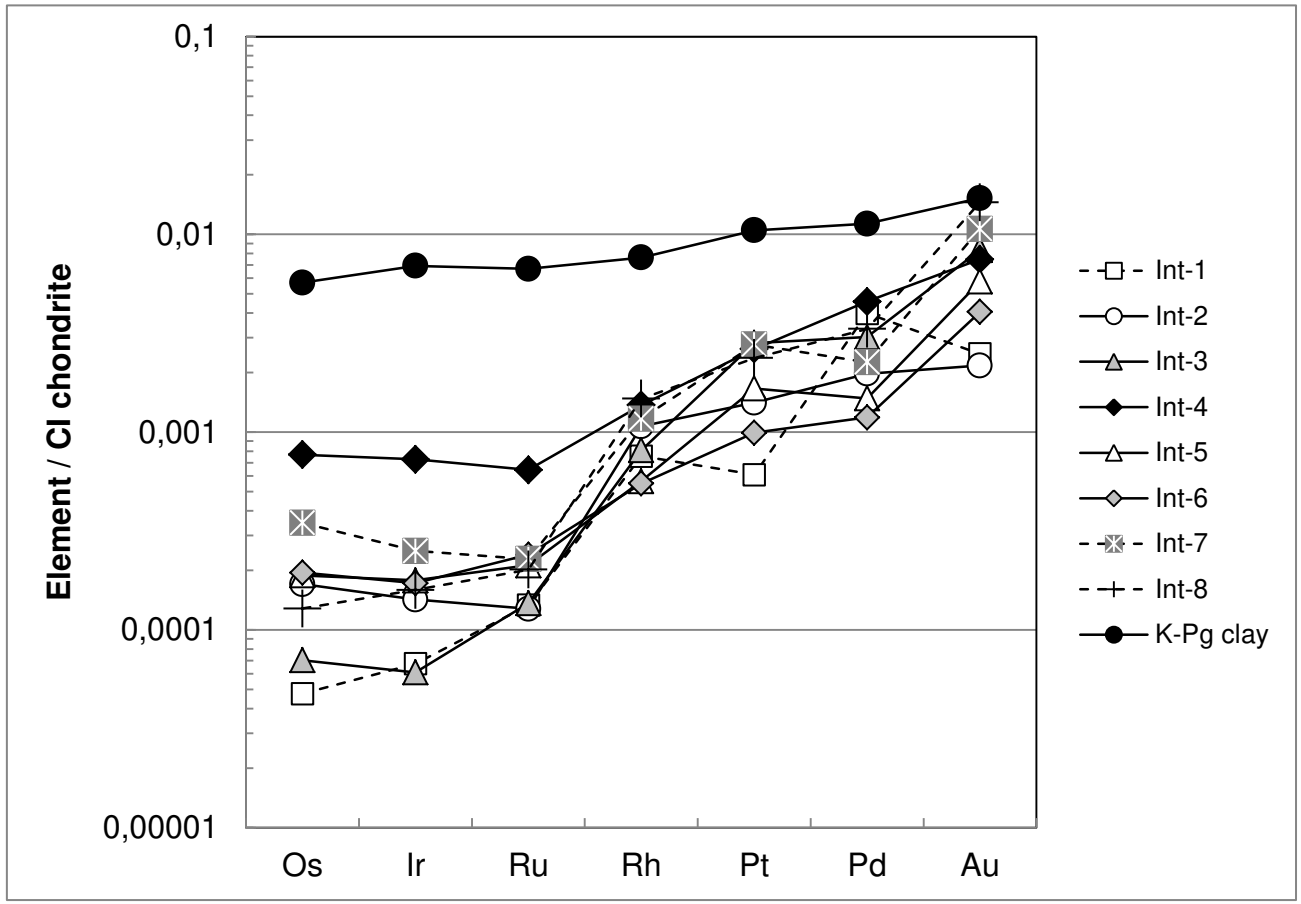

CI chondrite normalized
(Tagle and Berlin 2008)

	502 Os	472 Ir	717 Ru	135 Rh	959 Pt	563 Pd	139 Au
Int-1	4,76E-05	6,75E-05	1,33E-04	7,55E-04	6,08E-04	3,99E-03	2,49E-03
Int-2	1,70E-04	1,42E-04	1,28E-04	1,07E-03	1,41E-03	1,97E-03	2,17E-03
Int-3	7,02E-05	6,10E-05	1,36E-04	8,10E-04	2,82E-03	3,02E-03	8,34E-03
Int-4	7,69E-04	7,29E-04	6,44E-04	1,37E-03	2,63E-03	4,57E-03	7,48E-03
K-Pg clay	5,70E-03	6,93E-03	6,69E-03	7,63E-03	1,05E-02	1,13E-02	1,53E-02
Int-5	1,89E-04	1,78E-04	2,12E-04	5,65E-04	1,66E-03	1,48E-03	5,78E-03
Int-6	1,95E-04	1,72E-04	2,40E-04	5,50E-04	9,93E-04	1,19E-03	4,05E-03
Int-7	3,47E-04	2,51E-04	2,28E-04	1,17E-03	2,77E-03	2,26E-03	1,07E-02
Int-8	1,28E-04	1,59E-04	2,01E-04	1,48E-03	2,37E-03	3,33E-03	1,45E-02

Chondrite normalised PGE ratios

	[Os/Ir]N	[Ru/Ir]N	[Rh/Ir]N	[Pt/Ir}N	[Pd/Ir]N	[Ru/Rh]N
Int-1	0,71	1,97	11,19	9,02	59,10	0,18
Int-2	1,20	0,90	7,51	9,90	13,87	0,12
Int-3	1,15	2,24	13,29	46,32	49,59	0,17
Int-4	**1,05**	**0,88**	**1,88**	**3,60**	**6,28**	**0,47**
K-Pg clay	**0,82**	**0,97**	**1,10**	**1,51**	**1,63**	**0,88**
Int-5	1,06	1,19	3,18	9,34	8,33	0,38
Int-6	1,13	1,39	3,19	5,76	6,89	0,44
Int-7	1,39	0,91	4,66	11,06	9,00	0,19
Int-8	0,81	1,27	9,27	14,88	20,89	0,14

0,63	0,754317
0,75	0,898589
0,78	0,934902
0,29	0,344347
0,74	0,890167
0,83	0,997595
0,88	1,052635
0,62	0,743591
0,57	0,689753